Nanoscale

RSC Publishing

PAPER

Rapid two-step metallization through physicochemical conversion of Ag_2O for printed "black" transparent conductive films

Cite this: *Nanoscale*, 2013, **5**, 5043

Dong-Youn Shin,[a] Gi-Ra Yi,[b] Dongwook Lee,[c] Jungwon Park,[c] Young-Boo Lee,[d] Inseok Hwang[c] and Sangki Chun*[c]

A rapid two-step metallization for fabrication of a "black" transparent conductive film on a flexible substrate for display applications is presented, using a mixture of silver oxide (Ag_2O) and silver neodecanoate ($C_{10}H_{19}AgO_2$), and its electrical conductivity and colour transition behaviours are investigated. Silver nanoparticles, which are physicochemically converted from silver oxide microparticles in the presence of silver neodecanoate in the course of the first metallization step at 150 °C for 10 min, are chemically annealed by immersing them in an acidic ferric chloride ($FeCl_3$) solution at room temperature for 10 s. During this second metallization step, silver nanoparticles are found to be tightly packed through Ostwald ripening, which eventually leads to the dramatic enhancement of electrical conductivity by six orders of magnitude from 1.33 S m^{-1} to 1.0 × 10^7 S m^{-1}, which corresponds to 15.9% of the electrical conductivity of bulk silver. In addition to the enhancement of electrical conductivity, the silver chloride (AgCl) layer formed on the surface of the silver layer due to ferric ions (Fe^{3+}) enhances the blackness of the transparent conductive film by a factor of 1.69, from 36.29 B to 61.51 B. The sheet resistance and optical transparency of a roll-to-roll printed black transparent conductive film for a touch screen panel are found to be as low as 0.9 Ω $\square^{-1}$ and 81%, respectively, after conducting the proposed two-step metallization.

Received 24th February 2013
Accepted 1st April 2013

DOI: 10.1039/c3nr00962a

www.rsc.org/nanoscale

1 Introduction

Printing techniques have been actively explored with a view of fabricating cheap, highly conductive electrodes at high resolution because of their huge potential for application in flexible electronics and display appliances such as transparent film heaters,[1] transistor circuits,[2–6] radio frequency identification (RFID) tags,[7] electromagnetic wave interference (EMI) shielding films[8] and other potential applications.[9–11] Among the various potential appliances, flexible touch screen panels (TSPs) have gained significant industrial interest due to the significant rise in market demand due to the advent of smart phones and tablet PCs.

A capacitive type of TSP, which conventionally uses a set of indium tin oxide (ITO) deposited substrates, has become the most commercially dominant among other types of TSPs, and its size could be enlarged from 4 inches for handheld smart phones through 10 inches for tablet PCs to 40 inches and above for public displays, as human nature is more and more adapted to touching displays rather than using other means of selecting information such as a computer mouse. However, the use of ITO increases the cost of producing TSPs while its low electrical conductivity poses an obstacle to the production of ultra-large TSPs, such as those used in public displays or electronic whiteboards.

Therefore, the development of ultra-large TSPs printed with a highly conductive but low-temperature processable paste (>10^4 S cm^{-1}) *in lieu* of ITO has been a significant issue because low-cost flexible substrates – such as polyethylene terephthalate (PET, T_g = 80 °C, where T_g stands for glass transition temperature), polycarbonate (PC, T_g = 145 °C), and polyethylene naphthalate (PEN, T_g = 150 °C)[12] – cannot withstand the conventional sintering temperature, which can be as high as 200 °C and above.[13,14] As an example, a conductive paste in a mixed form of silver oxide (Ag_2O) and silver carboxylate (RCOOAg, where R is an alkyl group) was found to be suitable for producing highly conductive patterns by a thermal reduction process at a temperature as low as 150 °C.[15,16] However, this thermal reduction process requires at least half an hour, which eventually leads to an increase of the overall fabrication cost due to its very poor productivity.

[a]*Department of Graphic Arts Information Engineering, Pukyong National University, Yongdang-dong, Nam-gu, Busan, 608-739, Republic of Korea. E-mail: dongyoun.shin@gmail.com; Fax: +82-51-629-6388; Tel: +82-51-629-6394*

[b]*Department of Engineering Chemistry, Chungbuk National University, Cheongju, Chungbuk 361-763, Republic of Korea. E-mail: yigira@chunbuk.ac.kr*

[c]*Information and Electronic Materials Institute, LG Chem Research Park, Daejeon, 305-380, Republic of Korea. E-mail: touchlee@lgchem.com; garden@lgchem.com; ishwang@lgchem.com; sangki@lgchem.com; Fax: +82-42-861-2056; Tel: +82-42-866-5992*

[d]*Korea Basic Science Institute, Jeonju, 561-756, Republic of Korea. E-mail: yblee@kbsi.re.kr*

To shorten the sintering time required to reach sufficiently high electrical conductivity as well as to lower the sintering temperature, various sintering techniques have been explored. As one of a number of dry sintering techniques, laser sintering has been introduced for the fast transformation of as-printed non-conductive silver lines into conductive ones.[17,18] However, this not only requires a highly expensive high-power laser system but also tends to produce non-uniform silver lines. Other dry sintering techniques such as microwave,[19,20] plasma,[21] and pulsed light[22,23] have also been developed, with which highly conductive silver lines can be produced more quickly. To further enhance the final electrical conductivity of dry sintered metallic parts, combinations such as pulsed light and microwave, or plasma and microwave, were also explored,[24,25] and it was found that up to 60% of the electrical conductivity of bulk silver could be achieved. However, plasma sintering requires an expensive inert gas such as argon for the ignition and retention of plasma, which could pose a significant cost barrier to the production of cheap, transparent, conductive films. Microwave sintering not only requires a special chamber to confine microwave irradiation but also needs to satisfy the special relationship between microwave frequency and line length to be sintered.[25] Despite the achievement of highly conductive transparent films without direct thermal sintering, however, these non-thermal dry sintering techniques still require more room to develop for an open continuous roll-to-roll process, which is desirable for the mass production of cheap, transparent, conductive films.

As an alternative approach to the aforementioned dry sintering techniques, wet sintering techniques on the basis of a chemical reaction have been proposed, which include the use of reducing agents for the reduction of metal precursors ($NaBH_4$ for the reduction of copper citrate),[26] combinatorial exposure to UV light and hydroquinone solution for the reduction of a silver metallo-organic compound,[27] vapour of ethylene glycol or 1-dimethylamino-2-propanol for the reduction of silver nitrate,[28,29] a destabilizing agent (NaCl) for the self-sintering of silver nanoparticles,[30] and various electrolyte solutions ($CaCl_2$, HCl, LiCl, $MgCl_2$, NaCl, $FeSO_4$, and $MgSO_4$) for the chemical sintering of silver nanoparticles.[31,32]

Wet sintering techniques, especially using electrolyte solutions, have strong advantages over other non-thermal dry sintering techniques in the sense that they do not require special equipment yet can achieve high electrical conductivity up to 40% within 10 s (ref. 30 and 32). These advantages certainly make wet sintering techniques more amenable to an open continuous roll-to-roll process. However, previous research in this field has focused only on enhancing the electrical conductivity of as-printed metallic parts. In practical display applications including touch screen panels, the blackness of silver electrodes is of significant concern, but this issue was not considered in previous research. As shown in Fig. 1, a transparent conductive film with reflective silver electrodes not only deteriorates the display contrast ratio but also contributes to colour mismatching in the specified colour spectrum as well as the haziness of a transparent conductive film when viewed at a glancing angle. Especially, the haziness of a transparent conductive film is a significant reason why transparent conductive films with silver nanowires have not been readily commercialized despite the relative ease with which they can be manufactured.[33–35] In addition to the need to suppress the metallic reflection of silver electrodes, they also need to be covered by a topmost protection layer against their unwanted oxidation during O_2 plasma treatment,[36] which would have to be adopted in the fabrication of most types of displays.

In order to meet all the aforementioned requirements such as low-temperature processability, short processing time, high electrical conductivity and low reflectivity with a protection layer, a novel two-step metallization has been devised for the purpose of this research, whereby short thermal sintering is applied first, followed by a wet sintering technique with an aqueous ionic solution. The physicochemical conversion of silver oxide microparticles to silver nanoparticles in the presence of silver neodecanoate during the first metallization step and the effect of ions on the enhancement of electrical conductivity, blackness and formation of a protective layer during the second metallization step will be comprehensively discussed.

2 Experimental

2.1 Sample preparations

The silver oxide paste was prepared by mixing silver oxide microparticles (D50 ≈ 1.89 μm, Kojundo Chemical Laboratory

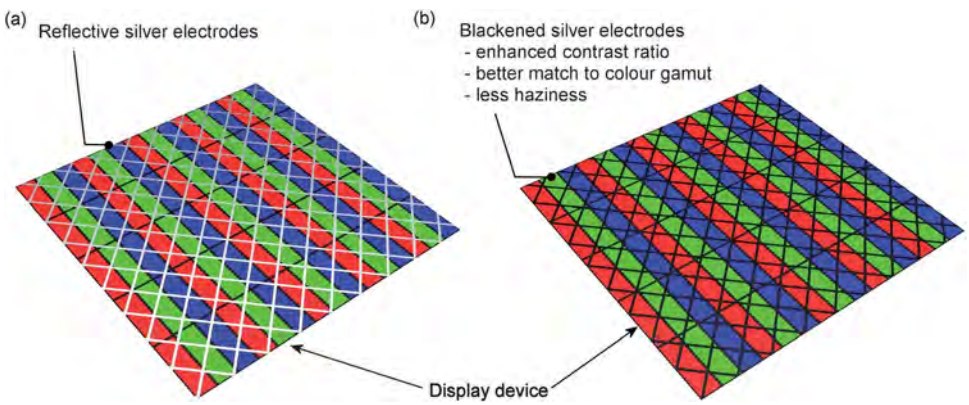

Fig. 1 Visual impact of transparent conductive films with (a) reflective silver electrodes and (b) blackened silver electrodes.

Co. Ltd, Japan) and silver neodecanoate ($C_{10}H_{19}AgO_2$) in α-terpineol ($C_{10}H_{18}O$, Kanto Chemical Co. Inc., Japan) at a specified weight ratio of 2 : 2 : 1, respectively. All the components were pre-mixed for 2 min and degassed for 1 min using a planetary centrifugal mixer (AR-250, Thinky Corp., Japan), followed by a triple roller mill (EXAKT 50, EXAKT Advanced Technologies GmbH, Germany) to break down any remaining large agglomerates of silver oxide microparticles.

Various aqueous ionic solutions were prepared with hydrochloric acid (HCl, Sigma-Aldrich Co. LLC., USA), sodium chloride (NaCl, Sigma-Aldrich Co. LLC., USA), ferrous chloride ($FeCl_2$, Kanto Chemical Co. Inc., Japan), ferric chloride ($FeCl_3$, Kanto Chemical Co. Inc., Japan), ferrous acetate ($Fe(C_2H_3O_2)_2$, Sigma-Aldrich Co. LLC., USA), and ferrous sulphate ($FeSO_4$, Kanto Chemical Co. Inc., Japan) without further purification.

The silver oxide paste was bar-coated using a four-sided applicator (PA-2020, BYK-Gardner GmbH, Germany) on a PET film with a thickness of 30 μm, and then thermally sintered at 150 °C for 10 min in the first metallization step, by which the silver oxide paste was dried and endowed with adhesive strength as well as initial conductivity. In the second metallization step, the bar-coated silver oxide paste was immersed in aqueous ionic solutions for 10 s, followed by washing with deionized water twice and drying under ambient conditions.

2.2 Characterizations

The differential scanning calorimetric (DSC) thermograms of the silver oxide paste with and without silver neodecanoate were characterized with a thermal analyser (DSC 823e, Mettler-Toledo GmbH, Germany) at a heating rate of 10 °C min^{-1} and a dry air flow rate from 25 to 30 ml min^{-1}. A four-point probe (MCP-T600, Mitsubishi Chemical Corp., Japan) was used to measure the surface electrical resistance of the silver films made with the silver oxide paste. The thickness of the silver films was measured using a Teclock dial indicator according to Japanese Industrial Standards (JIS, K6783). The optical reflectivity of the silver films was measured using a UV-VIS-NIR spectrophotometer (UV-3600, Shimadzu Corp., Japan). The morphological characterization of the silver films was performed with a field emission scanning electron microscope (FE-SEM) (S-4800, Hitachi High-Technologies Corp., Japan). An X-ray photoelectron spectroscope (XPS) (ESCALAB 250, Thermo Scientific Inc., USA) with a monochromatized Al Kα X-ray (1486.6 eV) source was employed to analyse the chemical composition of the silver films before and after rapid chemical annealing with aqueous ionic solutions.

3 Results and discussion

3.1 Physicochemical conversion of the silver oxide paste during the first metallization step

The silver oxide paste initially had no silver nanoparticles. When the silver oxide paste with silver neodecanoate was exposed to short thermal sintering at around 150 °C in the first metallization step, however, a massive amount of silver nanoparticles was found to be produced within 10 min. Though part of them resulted from the thermal decomposition of silver

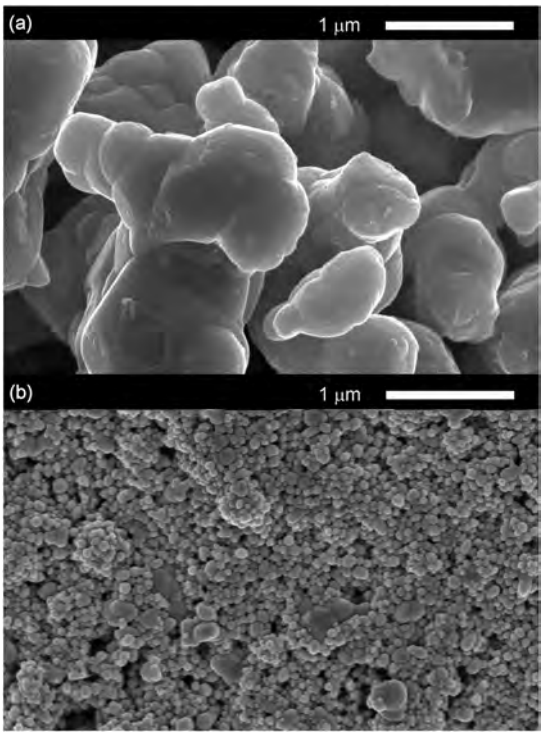

Fig. 2 Impact of silver neodecanoate on the formation of silver nanoparticles during the first metallization step at 150 °C for 10 min. (a) Silver oxide microparticles alone and (b) silver oxide microparticles with silver neodecanoate.

neodecanoate,[37] the silver oxide microparticles themselves were the major source of silver nanoparticles, as shown in Fig. 2.[15,38] The physicochemical conversion of silver oxide microparticles to silver nanoparticles in the presence of silver neodecanoate not only lowers the chemical reduction temperature of silver oxide to silver from 400 °C in the case of silver oxide alone to 180 °C in the case of silver oxide with silver neodecanoate, but also leads to an exothermic chemical reaction, as shown in Fig. 3. This physicochemical reduction, however, might be impeded by the use of a dispersant so that the use of silver oxide

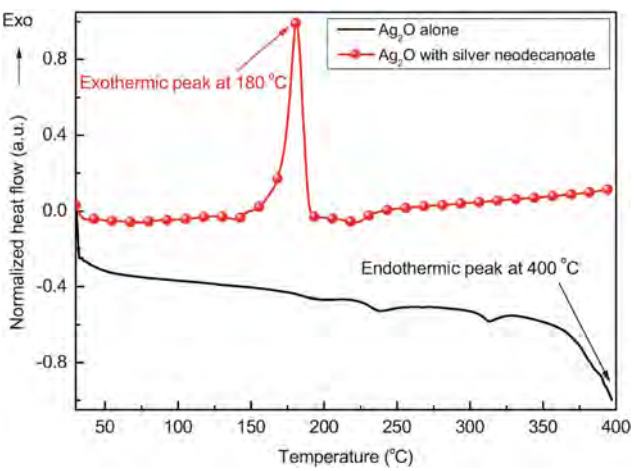

Fig. 3 DSC thermograms of silver oxide alone and silver oxide with silver neodecanoate.

microparticles rather than silver oxide nanoparticles is preferable so as to have fewer agglomerates in the silver oxide paste in the absence of the dispersant.

The electrical conductivity of the silver oxide paste, along with the thermal sintering time at 150 °C, was found to evolve from 1.33 S m^{-1} in 10 min through 2.52 × 10^6 S m^{-1} in 15 min to 6.79 × 10^6 S m^{-1} in 30 min, as shown in Fig. 4(a). However, the average crystalline size of the silver nanoparticles, which was calculated from the XRD patterns in Fig. 4(b) using the Scherrer equation based on the fundamental parameter approach (Rietveld refinement) with the TOPAS software,[39–42] was found to remain almost the same, at 35 nm, regardless of the thermal sintering time at the applied sintering temperature. This means that the fusion of silver nanoparticles takes place only at the interface of the silver nanoparticles through atomic diffusion, but is not strong enough to completely merge the silver nanoparticles together. The preservation of silver nanoparticles formed from the silver oxide paste during the first metallization step plays a vital role in realizing the second metallization step with aqueous ionic solutions, which will be discussed in the next section.

3.2 Enhancement of electrical conductivity and blackness at the second metallization step

Although bulk silver has little chemical reactivity to aqueous ionic solutions, it is reported in the relevant literature that the chemical reactivity of silver to aqueous ionic solutions can be greatly enhanced when the size of the silver nanoparticles is smaller than 10 nm.[43] Therefore, the formation and preservation of silver nanoparticles converted from silver oxide microparticles in the first metallization step might significantly contribute to the promotion of rapid chemical annealing in the second metallization step. However, the silver nanoparticles formed in the first metallization step were sized about 35 nm, which is 3.5 times larger than the size of the silver nanoparticles reported in the literature, so their chemical reactivity to aqueous ionic solutions needs to be re-assessed by immersing the silver films produced in the first metallization step into various aqueous ionic solutions such as hydrogen chloride (HCl, pH = 1.43), 6 wt% of sodium chloride (NaCl, pH = 5.8), 6 wt% of ferrous chloride ($FeCl_2$), 6 wt% of ferric chloride ($FeCl_3$), 6 wt% of ferrous acetate ($Fe(C_2H_3O_2)_2$), 6 wt% of ferrous sulphate ($FeSO_4$), and a mixture of 6 wt% of ferrous sulphate and 6 wt% of sodium chloride. It should be noted that 6 wt% of sodium chloride was used to investigate whether the low pH condition is vital for rapid chemical annealing in the second metallization step.

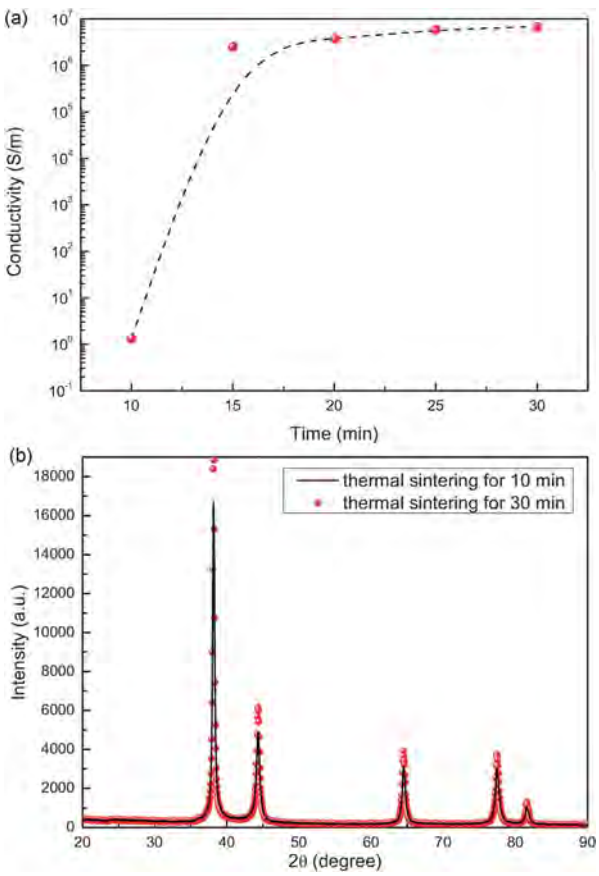

Fig. 4 Impact of thermal sintering time at 150 °C on (a) electrical conductivity and (b) silver crystalline size after 10 min and 30 min.

In the presence of chloride ions (Cl^-) and dissolved oxygen in water at a low pH condition, the silver nanoparticles formed in the first metallization step can be dissolved slowly into silver ions (Ag^+).[44–46] The redox reaction in this case can be written as $4Ag + O_2 + 2H_2O \leftrightarrow 4Ag^+ + 4OH^-$, where the reduction potential of O_2/OH^- is 0.4 V.[47] Since molecular oxygen adsorbs and dissociates to atomic oxygen on the silver surface between 200 K and 500 K,[48] atomic oxygen on the silver surface may block the re-deposition of silver ions onto the silver surface. Since the concentration of oxygen in water is quite limited and the adsorption process is dynamically equilibrated, however, there is still a good chance that a small amount of silver ions can be re-deposited onto the relatively more active silver surface.

As a consequence, rapid chemical annealing with various aqueous ionic solutions, regardless of their pH condition, results in an increase of crystallinity from 35 nm to 45 nm in the case of hydrogen chloride, sodium chloride, ferrous chloride, and a mixture of ferrous sulphate and sodium chloride, as shown in Fig. 5(a)–(f). In the case of ferric chloride, the crystalline size of the silver nanoparticles was found to increase up to 50 nm, and a strong network of silver nanoparticles was formed. Their resulting conductivity values after the second metallization step were greatly improved by factors of 1.13 × 10^7 in the case of hydrogen chloride, 1.2 × 10^7 in the case of sodium chloride, 3.09 × 10^6 in the case of ferrous chloride, and 7.54 × 10^6 in the case of ferric chloride, as shown in Fig. 6.

On the other hand, two non-chloride aqueous ionic solutions, ferrous acetate and ferrous sulphate, were found to lack the ability to fuse silver nanoparticles, resulting in their silver crystalline sizes remaining unchanged and virtually no enhancement of their electrical conductivity. It was only when sodium chloride was added to a non-chloride aqueous ionic solution, for example, a mixture of ferrous sulphate and sodium chloride, the electrical conductivity of the silver film was increased by a factor of 5.20 × 10^6, as shown in Fig. 6. Therefore, it is confirmed that chloride ion is the key to dramatically

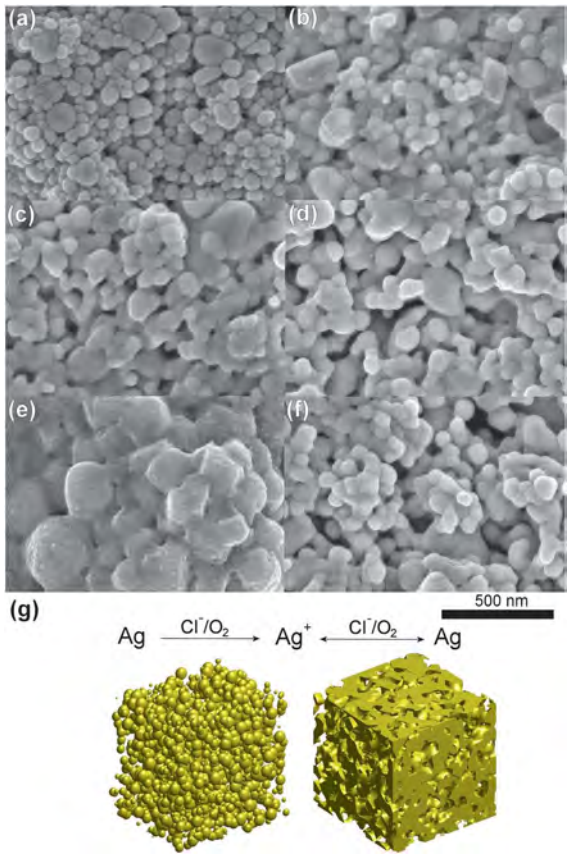

Fig. 5 SEM images of the silver films just after the first metallization step in (a), and after the second metallization step with (b) HCl, (c) NaCl, (d) $FeCl_2$, (e) $FeCl_3$, and (f) $FeSO_4$ + NaCl. Schematic illustration of the self-catalytic addition of silver ions to the silver film in (g).

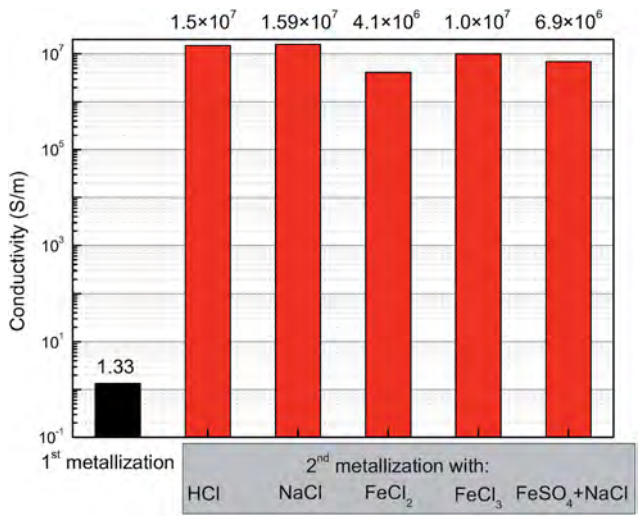

Fig. 6 Enhancement of electrical conductivity in the second metallization step with various aqueous ionic solutions.

enhance the electrical conductivity of the silver films in the second metallization step.[30,32] This enhancement of the electrical conductivity of the silver films chemically annealed with aqueous ionic solutions containing chloride ions is led by the self-catalytic addition of dissolved silver ions on the surface of the silver nanoparticles, as shown in Fig. 5(g). This self-catalytic addition is facilitated by the silver nanoparticles formed and preserved in the first metallization step through Ostwald ripening.[21,24] It is noteworthy that the enhancement of the electrical conductivity of the silver film chemically annealed with ferric chloride basically follows the self-catalytic addition similar to that shown in Fig. 5(g), but involves another chemical reaction, which will be discussed later in detail.

Although the electrical conductivity of the silver films was dramatically enhanced after chemical annealing in the course of the second metallization step with aqueous ionic solutions containing chloride ions, especially with hydrogen chloride and sodium chloride, they still exhibited metallic reflection, with the exception of the silver film chemically annealed with ferric chloride, which showed the intended blackening of the silver film. The XRD spectra of the silver films revealed that the formed black layer, after rapid chemical annealing with ferric chloride, was silver chloride (AgCl), as shown in Fig. 7.

Unlike Ki and Zhu's work,[43] however, no chlorine peaks of silver chloride were detected in the XRD spectra of the silver films chemically annealed with hydrogen chloride, sodium chloride, ferrous chloride and a mixture of ferrous sulphate and sodium chloride. This means that the formed silver nanoparticles were too big to have sufficient chemical reactivity for the formation of silver chloride within such a short chemical annealing time. Moreover, they contained only chloride ions without a suitable electron acceptor.

On the other hand, an aqueous ferric chloride solution contains a strong electron acceptor, ferric ion (Fe^{3+}), which contributes to the formation of silver chloride.[49–51] It was also found that the chemical reactivity of a silver particle, which is inversely proportional to its size, is not a prerequisite to the formation of silver chloride with the presence of ferric ions. As shown in Fig. 8, three aqueous ionic solutions, hydrogen chloride, sodium chloride and ferric chloride, which exhibited good electrical conductivity of more than 1.0×10^7 S m^{-1}, were applied to the first sintered silver films composed of different

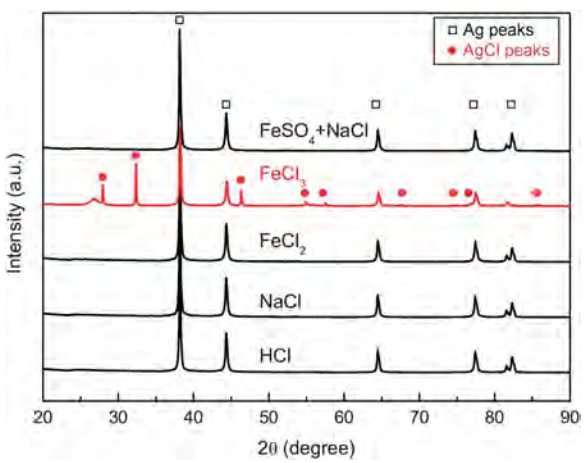

Fig. 7 XRD spectra of the silver films chemically annealed with HCl, NaCl, $FeCl_2$, $FeCl_3$, and $FeSO_4$ + NaCl.

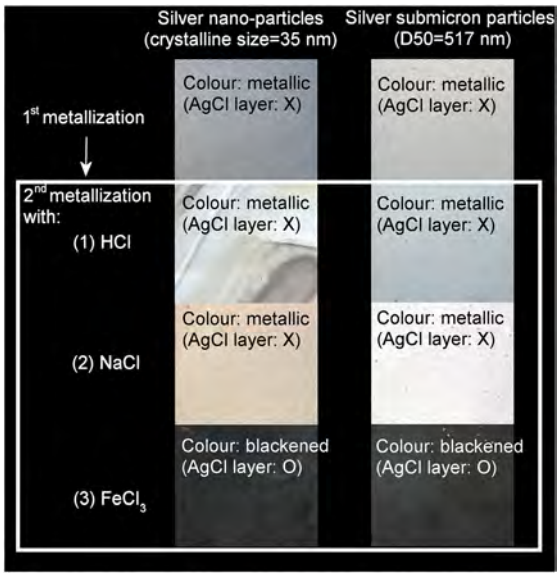

Fig. 8 Capability of ferric ions (Fe^{3+}) for the formation of silver chloride on the silver films with different sizes of silver particles.

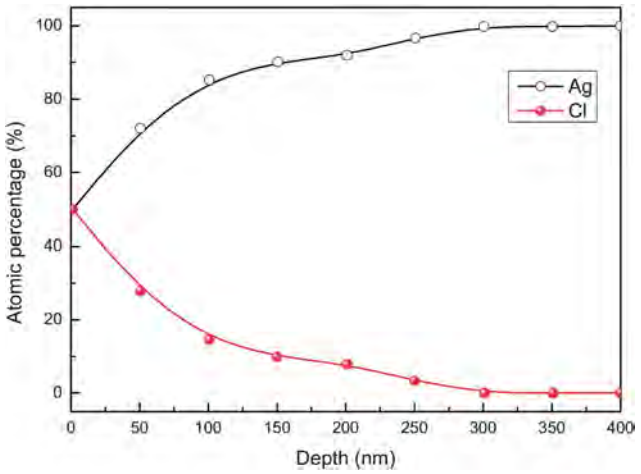

Fig. 9 Depth profile of the atomic ratio of chlorine to silver in the silver film chemically annealed with $FeCl_3$.

silver particles, 35 nm and 517 nm. Among them, only the aqueous ferric chloride solution successfully formed silver chloride, irrespective of the sizes of the silver particles.

Compared to the silver films chemically annealed with the other chloride containing aqueous ionic solutions, the crystalline size of the silver nanoparticles of the silver film chemically annealed with ferric chloride was found to be further enlarged up to 50 nm. This may have been caused by the re-deposition of more silver ions on the silver surface through the redox reaction of ferric ions. The enlarged crystalline size of the silver nanoparticles may have contributed to the higher electrical conductivity of the silver film, but the measured electrical conductivity of the silver film chemically annealed with ferric chloride was slightly lower than those chemically annealed with hydrogen chloride and sodium chloride.

This may have been caused by the formation of non-conductive silver chloride, whose crystalline size was measured up to 170 nm. If silver chloride was formed all through the depth of the silver film, however, the silver film chemically annealed with ferric chloride would become non-conductive. Therefore, it could be postulated that the self-catalytic addition of silver ions to the silver film to enhance electrical conductivity must proceed much faster than the formation of silver chloride, and that the formed silver chloride layer must stay only on the upper part of the silver film. This means that the oxidation of silver nanoparticles to silver chloride must start from the interface in contact with the ferric chloride solution, penetrate to the depth of the silver film, and finally stop somewhere before the entire transformation of the silver film into silver chloride.

Using X-ray photon spectroscopy, this postulation was confirmed in which the atomic ratio of chlorine to silver gradually decreases with increasing depth and then disappeared at around 300 nm depth, as shown in Fig. 9. The chemical composition of silver to silver chloride in the silver film chemically annealed with ferric chloride was measured using the Rietveld refinement of X-ray diffraction spectra and was found to be 7 : 3. Using the morphological images and depth profile data of the atomic percentages shown in Fig. 2, 5 and 9, the overall physicochemical reactions involved with the silver film in the first and second metallization steps with ferric chloride are re-constructed in Fig. 10.

As shown in Fig. 11(a), the reflectivity of the silver film was reduced over the entire visible range from 400 nm to 700 nm, regardless of the chemical annealing time with ferric chloride, and hence the haziness of the silver film was reduced. The degree of blackness (B) of the silver film is defined by $116(1 - Y^{1/3})$ when the optical reflectivity at 550 nm, Y, is greater than 0.008856, rather than the average reflectivity over the entire visible range,[52] because the most perceptive wavelength of light to the human eye is around 550 nm.[53,54]

When the silver film was chemically annealed with ferric chloride, the silver film quickly blackened in 10 s from 36.29 B to 61.51 B with the simultaneous enhancement of electrical conductivity due to the increase in the crystalline size of the silver nanoparticles from 35 nm to 50 nm. However, the prolonged immersion time up to 50 s did not notably enhance the blackness of the silver film, but it did adversely decrease its electrical conductivity, as shown in Fig. 11(b). This adverse deterioration in electrical conductivity with the prolonged immersion time resulted from the gradual increase of the thickness of the non-conductive silver chloride layer formed on the surface of the silver film, as discussed before.

Silver chloride is a photosensitive material, which can be decomposed into silver nanoparticles and chlorine gas upon exposure to light because of point ionic defects and electron traps under UV and visible light.[55] This photodecomposition mechanism has been used in photography for centuries, and the formed silver nanoparticles contribute to the blackening of the region exposed to light. However, the silver film chemically annealed with ferric chloride was found to preserve silver chloride from photodecomposition, as shown in Fig. 7 and 9. This unusual stability of silver chloride results from the pairing

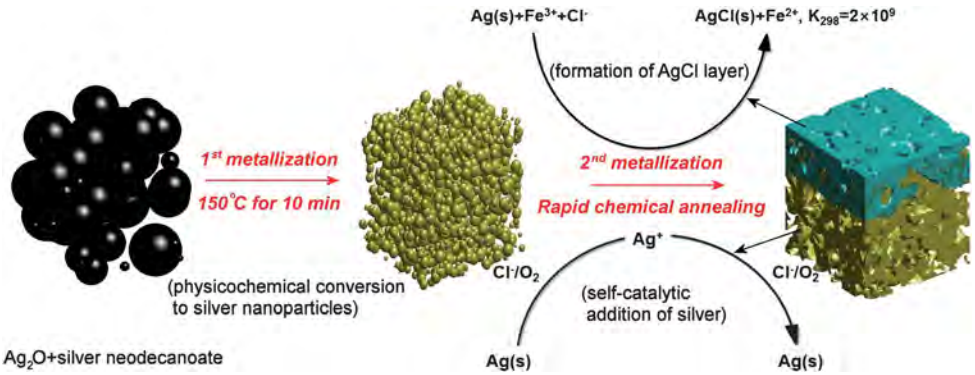

Fig. 10 Schematic illustration of the overall physicochemical reactions in the course of low-temperature two-step metallization with $FeCl_3$.

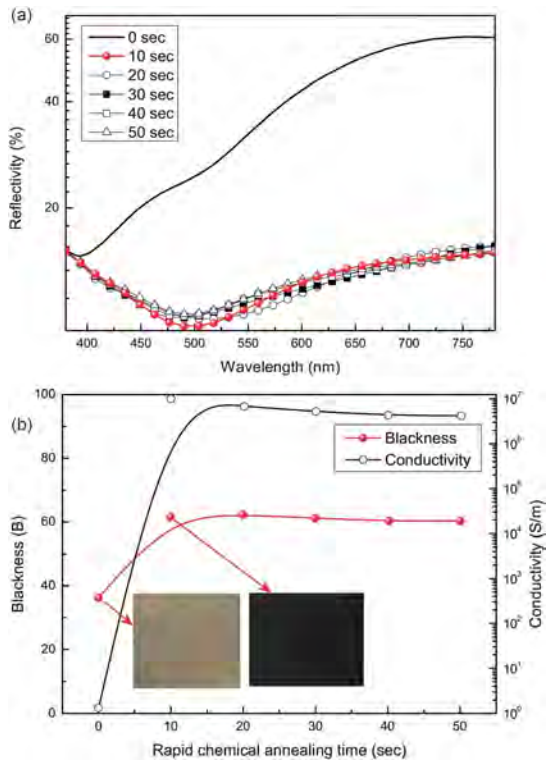

Fig. 11 Optical properties of the silver film chemically annealed with $FeCl_3$. (a) Reflectivity and (b) blackness and electrical conductivity of the silver film.

of silver chloride with silver nanoparticles. Light is strongly absorbed by silver nanoparticles *via* surface plasmon resonance, depending on their size and shape,[56,57] instead of silver chloride. The photons absorbed by silver nanoparticles are separated into electrons and holes. Then, the electrons are transferred to the surface of the silver nanoparticles farthest from the silver/silver chloride interface, rather than to the silver ions of the silver chloride lattice.[58,59] As a result, the silver chloride remained intact under light illumination.

However, the blackness of the silver film after the chemical annealing with ferric chloride might not be explained solely with the surface plasmon resonance of silver nanoparticles. In fact, silver nanoparticles were present in the silver film even before the chemical annealing with ferric chloride, but the colour of the silver film exhibited a metallic reflection. To investigate the role of the silver chloride layer, therefore, the topmost silver chloride layer was removed with an ammonium hydroxide (NH_4OH) solution (1 M) for 1 min, as shown in Fig. 12, and the colour of the silver film without the silver chloride layer was again found to exhibit a metallic reflection. This supports the idea that the formation of a silver/silver chloride heterostructure not only preserves silver chloride from photodecomposition but also contributes to the blackness of the silver film due to the enhanced surface plasmon resonance.[60]

3.3 Black transparent conductive films for touch screen panels

The proposed two-step metallization process can be readily applied to real TSPs because it satisfies all the required characteristics for printed ultra-large TSPs, including low-temperature processability, a short processing time, high electrical

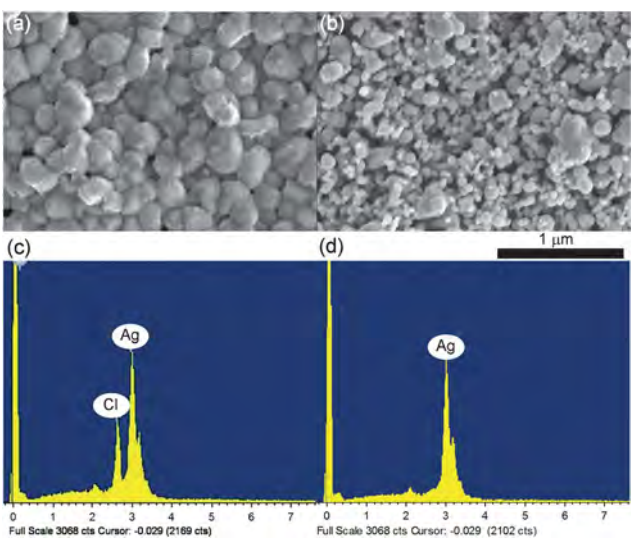

Fig. 12 SEM images and EDX spectra of the Ag/AgCl heterostructure formed by rapid chemical annealing with $FeCl_3$ for 10 s in (a) and (c), and the underlying silver nanoparticles after selective removal of AgCl with NH_4OH in (b) and (d).

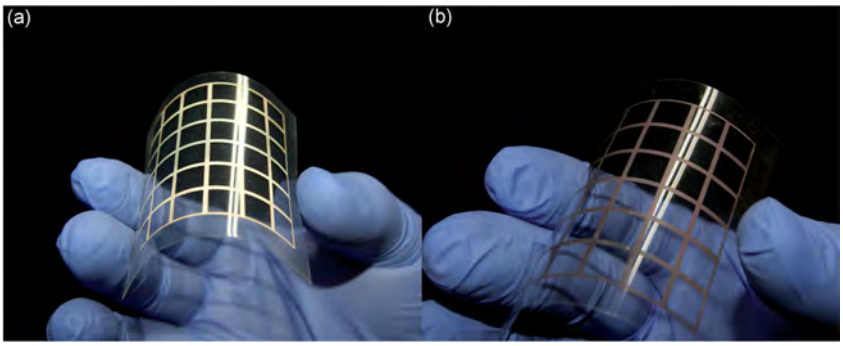

Fig. 13 Visual impact comparison of silver electrodes, (a) just after the first metallization step and (b) after the second metallization step for blackened electrodes with $FeCl_3$.

conductivity, and low reflectivity. The first metallization step physicochemically converts silver oxide microparticles into silver nanoparticles in the presence of silver neodecanoate at a temperature as low as 150 °C for 10 min. Simultaneously with the electrical conductivity enhancement through self-catalytic addition, the colour of the square mesh electrodes blackened in the course of the second metallization step with ferric chloride at room temperature in 10 s. The visual impact of the black transparent conductive film becomes obvious, when compared to a conventional transparent conductive film with reflective silver electrodes, as shown in Fig. 13, where the width of the square mesh electrodes was enlarged to 1 mm for the purpose of easy visual comparison at a distance.

Black transparent conductive films, whose square mesh electrodes were 3 μm thick, with a line width of 30 μm and a line pitch of 300 μm, were produced with a homemade roll-to-roll printing machine, as shown in Fig. 14(a). The chemical annealing time for the second metallization step was, however, extended to 30 s because of the limited operating conditions of the homemade roll-to-roll printing machine. The sheet resistance of the black transparent conductive film was 0.9 Ω $\square^{-1}$, which is still lower than that of the thermally sintered silver film for 20 min, 1.45 Ω $\square^{-1}$, but slightly higher than that of the thermally sintered silver film for 30 min, 0.68 Ω $\square^{-1}$. It is noteworthy that the enhancement of the sheet resistance of a black transparent conductive film is not as dramatic as that of the chemically annealed silver films in Fig. 6. This relatively poor enhancement of sheet resistance seems to have been caused by the formation of a thicker silver chloride layer not only on the top but also on the lateral sides of the electrodes during the extended chemical annealing time. Even under this harsh chemical annealing condition, however, the sheet resistance of the black conductive film was low enough for ultra-large TSPs.

We also investigated whether the silver chloride layer formed on the surface of the silver film could protect silver against oxidation when O_2 plasma treatment was applied for 10 min – something which would be adopted in the fabrication of most displays to enhance coatability in the subsequent production steps. The XRD spectra of the silver film covered with the silver chloride layer confirmed that oxidized silver was not formed after the O_2 plasma treatment, as shown in Fig. 14(b).

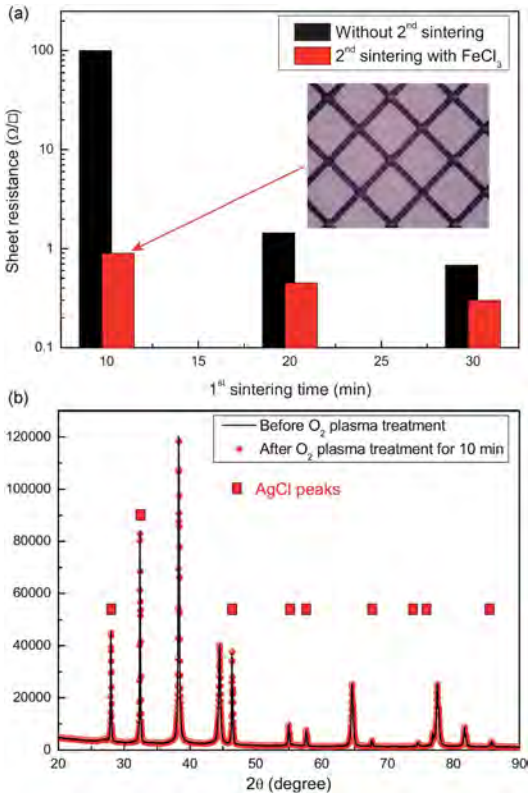

Fig. 14 Comparison of the sheet resistance of "black" transparent conductive films before and after chemical annealing with $FeCl_3$ for 30 s in (a) and the XRD spectra before and after O_2 plasma treatment in (b).

4 Conclusions

We have demonstrated the applicability of a low-temperature processable two-step metallization with a silver oxide paste to construct black square mesh electrodes for touch screen panels. The developed silver oxide paste was mainly composed of silver oxide microparticles, the average size of which was around 1.89 μm, and silver neodecanoate ($C_{10}H_{19}AgO_2$) in α-terpineol ($C_{10}H_{18}O$). Short thermal sintering during the first metallization step physicochemically converted silver oxide microparticles to silver nanoparticles, the crystalline size of which was approximately 35 nm, in the presence of silver neodecanoate. This

exothermic physicochemical conversion of the silver oxide paste eventually contributed to lowering the initial sintering temperature to as low as 150 °C and to shortening the sintering time to as little as 10 min.

In order to enhance the electrical conductivity and blackness of the silver film, rapid chemical annealing with diverse aqueous ionic solutions was performed for 10 s in the second metallization step. Among the several anions used here, chemical annealing with chloride ions was found to be the most effective in enhancing the electrical conductivity of the silver film through the self-catalytic addition of silver ions to the silver film, resulting in the growth of the crystalline size of the silver nanoparticles through Ostwald ripening.

Moreover, the addition of electron donating ferric ions was found to be effective in producing silver chloride on the surface of the silver film only in 10 s, regardless of the size of the silver particles. The formation of a silver/silver chloride heterostructure contributes to the preservation of silver chloride from photodecomposition under light illumination as well as the blackness of the silver film due to the enhanced surface plasmon resonance. The silver chloride layer also works as a protective layer against the oxidation of silver during the subsequent O_2 plasma treatment.

In summary, a novel low-temperature processable two-step metallization has been found to be more amenable to an open continuous roll-to-roll process, which requires only a fraction of the usual metallization time, when compared to conventional thermal sintering processes. The blackened silver electrodes with the silver chloride layer in the second metallization step suppress the reflectivity of the silver electrodes and are thus suitable for use in a highly conductive transparent film for ultra-large TSPs, the sheet resistance of which is as low as 0.9 $\Omega\ \square^{-1}$ with an optical transparency of 81%.

Acknowledgements

Dong-Youn Shin was supported by the Basic Science Research Program through the National Research Foundation of Korea (NRF), which is funded by the Ministry of Education, Science and Technology (no. 2012R1A1A2038889). The author's gratitude is also extended to Hyuk Yu for his valuable discussions.

Notes and references

1 Y.-H. Yoon, J.-W. Song, D. Kim, J. Kim, J.-K. Park, S.-K. Oh and C.-S. Han, *Adv. Mater*, 2007, **19**, 4284.
2 H. E. Katz and J. Huang, *Annu. Rev. Mater. Res.*, 2009, **39**, 71.
3 Y. Li, Y. Wu and B. S. Ong, *J. Am. Chem. Soc.*, 2005, **127**, 3266.
4 Y. Wu, Y. Li and B. S. Ong, *J. Am. Chem. Soc.*, 2007, **129**, 1862.
5 J. Perelaer, C. E. Hendriks, A. W. M. de Laat and U. S. Schubert, *Nanotechnology*, 2009, **20**, 165303.
6 T. Sekitani, Y. Noguchi, U. Zschieschang, H. Klauk and T. Someya, *Proc. Natl. Acad. Sci. U. S. A.*, 2008, **105**, 4976.
7 H. Park, H. Kang, Y. Lee, Y. Park, J. Noh and G. Cho, *Nanotechnology*, 2012, **23**, 344006.
8 F. D. L. Vega, A. Garbar, C. Rottman, E. Masoud and B. Faulkner, *SID Int. Symp. Dig. Tech. Pap.*, 2006, **37**, 1987.
9 J. Weber, K. Potje-Kamloth, F. Haase, P. Detemple, F. Völklein and T. Doll, *Sens. Actuators, A*, 2006, **132**, 325.
10 R. Gaudiana and C. Brabec, *Nat. Photonics*, 2008, **2**, 287.
11 A. C. Siegel, S. T. Phillips, M. D. Dickey, N. Lu, Z. Suo and G. M. Whitesides, *Adv. Funct. Mater.*, 2009, **19**, 1.
12 M.-C. Choi, Y. Kim and C.-S. Ha, *Prog. Polym. Sci.*, 2008, **33**, 581.
13 H.-H. Lee, K.-S. Chou and K.-C. Huang, *Nanotechnology*, 2005, **16**, 2436.
14 J.-W. Park and S.-G. Baek, *Scr. Mater.*, 2006, **55**, 1139.
15 S. Chun, D. Grudinin, D. Lee, S.-H. Kim, G.-R. Yi and I. Hwang, *Chem. Mater.*, 2009, **21**, 343.
16 D.-Y. Shin, M. Jung and S. Chun, *J. Mater. Chem.*, 2012, **22**, 11755.
17 N. R. Bieri, J. Chung, S. E. Haferl, D. Poulikakos and C. P. Grigoropoulos, *Appl. Phys. Lett.*, 2003, **82**, 3529.
18 J. Chung, S. Ko, N. R. Bieri, C. P. Grigoropoulos and D. Poulikakos, *Appl. Phys. Lett.*, 2004, **84**, 801.
19 J. Perelaer, B.-J. de Gans and U. S. Schubert, *Adv. Mater*, 2006, **18**, 2101.
20 J. Perelaer, M. Klokkenburg, C. E. Hendriks and U. S. Schubert, *Adv. Mater*, 2009, **21**, 4830.
21 I. Reinhold, C. E. Hendriks, R. Eckardt, J. M. Kranenburg, J. Perelaer, R. R. Baumann and U. S. Schubert, *J. Mater. Chem.*, 2009, **19**, 3384–3388.
22 W.-S. Han, J.-M. Hong, H.-S. Kim and Y.-W. Song, *Nanotechnology*, 2011, **22**, 395705.
23 D. J. Lee, S. H. Park, S. Jang, H. S. Kim, J. H. Oh and Y. W. Song, *J. Micromech. Microeng.*, 2011, **21**, 125023.
24 J. Perelaer, R. Abbel, S. Wünscher, R. Jani, T. van Lammeren and U. S. Schubert, *Adv. Mater*, 2012, **24**, 2620.
25 J. Perelaer, R. Jani, M. grouchko, A. Kamyshny, S. Magdassi and U. S. Schubert, *Adv. Mater.*, 2012, **24**, 3993.
26 D. Li, D. Sutton, A. Burgess, D. Graham and P. D. Calvert, *J. Mater. Chem.*, 2009, **19**, 3719.
27 J. J. P. Valeton, Ko. Hermans, C. W. M. Bastiaansen, D. J. Broer, J. Perelaer, U. S. Schubert, G. P. Crawford and P. J. Smith, *J. Mater. Chem.*, 2010, **20**, 543.
28 J.-T. Wu, S. L.-C. Hsu, M.-H. Tsai and W.-S. Hwang, *Thin Solid Films*, 2009, **517**, 5913.
29 J.-T. Wu, S. L.-C. Hsu, M.-H. Tsai and W.-S. Hwang, *J. Phys. Chem. C*, 2011, **115**, 10940.
30 M. Grouchko, A. Kamyshny, C. F. Mihailescu, D. F. Anghel and S. Magdassi, *ACS Nano*, 2011, **5**, 3354.
31 S. Magdassi, M. Grouchko, O. Berezin and A. Kamyshny, *ACS Nano*, 2010, **4**, 1943.
32 Y. Long, J. Wu, H. Wang, X. Zhang, N. Zhao and J. Xu, *J. Mater. Chem.*, 2011, **21**, 4875.
33 S. De, T. M. Higgins, P. E. Lyons, E. M. Doherty, P. N. Nirmalraj, W. J. Blau, J. J. Boland and J. N. Coleman, *ACS Nano*, 2009, **3**, 1767.
34 L. Hu, H. S. Kim, J.-Y. Lee, P. Peumans and Y. Cui, *ACS Nano*, 2010, **4**, 2955.
35 A. R. Madaria, A. Kumar, F. N. Ishikawa, C. Zhou and C. Uniform, *Nano Res.*, 2010, **3**, 564.
36 J. M. Knight, R. K. Wells and J. P. S. Badyal, *Chem. Mater.*, 1992, **4**, 640.

37 A. L. Dearden, P. J. Smith, D.-Y. Shin, N. Reis, B. Derby and P. O'Brien, *Macromol. Rapid Commun.*, 2005, **26**, 315.
38 T. Morita, Y. Yasua, E. Ide and A. Hirose, *Mater. Trans.*, 2009, **50**, 226.
39 A. L. Patterson, *Phys. Rev.*, 1939, **56**, 978.
40 E. E. Finney and R. G. Finke, *J. Colloid Interface Sci.*, 2008, **317**, 351.
41 J. Zeng, X. Xia, M. Rycenga, P. Henneghan, Q. Li and Y. Xia, *Angew. Chem., Int. Ed.*, 2011, **50**, 244.
42 B. D. Cullity and S. R. Stock, in *Elements of X-ray Diffraction*, Prentice-Hall, Inc., New Jersey, USA, 3rd edn., 2001.
43 L. Ki and Y.-J. Zhu, *J. Colloid Interface Sci.*, 2006, **303**, 415.
44 B. Wiley, T. Harricks, Y. Sun and Y. Xia, *Nano Lett.*, 2004, **4**, 1733.
45 S.-H. Im, Y.-T. Lee, B. Wiley and Y. Xia, *Angew. Chem., Int. Ed.*, 2005, **117**, 2192.
46 B. Wiley, Y. Sun and Y. Xia, *Langmuir*, 2005, **21**, 8077.
47 T. Pal, T.-K. Sau and N. R. Jana, *Langmuir*, 1997, **13**, 1481.
48 F. Buatier de Mongeot, A. Cupolillo, U. Valbusa and M. Rocca, *Chem. Phys. Lett.*, 1997, **270**, 345.
49 H. Suzuki, T. Hirakawa, S. Sasaki and I. Karube, *Sens. Actuators, B*, 1998, **46**, 146.
50 H. R. Kim, Y. D. Kim, K. I. Kim, J. H. Shim, H. Nam and B. K. Kang, *Sens. Actuators, B*, 2004, **97**, 348.
51 B. J. Polk, A. Stelzenmuller, G. Mijares, W. MacCrehan and M. Gaitan, *Sens. Actuators, B*, 2006, **114**, 239.
52 N. Ohta and A. A. Robertson, in *Colorimetry: Fundamentals and Applications*, John Wiley & Sons, Inc., New York, USA, 2005.
53 T. H. Goldsmith, *Q. Rev. Biol.*, 1990, **65**, 281.
54 H. Tadashi, T. Taguchi and Y. Ueno, *US Pat.*, 4696548, 1987.
55 P. Wang, B. Huang, X. Qin, X. Zhang, Y. Dai, J. Wei and M.-H. Whangbo, *Angew. Chem., Int. Ed.*, 2008, **47**, 7931.
56 M. J. Mulvihill, X. Y. Ling, J. Henzie and P. Yang, *J. Am. Chem. Soc.*, 2010, **132**, 268.
57 T. Huang and X.-H. N. Xu, *J. Mater. Chem.*, 2010, **20**, 9867.
58 M. Choi, K.-H. Shin and J. Jang, *J. Colloid Interface Sci.*, 2010, **341**, 83.
59 Y. Zhu, H. Liu, L. Yang and J. Liu, *Mater. Res. Bull.*, 2012, **47**, 3452.
60 Y. Bi and J. Ye, *Chem. Commun.*, 2009, 6551.

